An Enhancement of Low-Frequency Variability in the Kuroshio–Oyashio Extension in CCSM3 owing to Ocean Model Biases

LUANNE THOMPSON

University of Washington, Seattle, Washington

YOUNG-OH KWON

Woods Hole Oceanographic Institution, Woods Hole, Massachusetts

(Manuscript received 31 August 2009, in final form 5 August 2010)

ABSTRACT

Enhanced decadal variability in sea surface temperature (SST) centered on the Kuroshio Extension (KE) has been found in the Community Climate System Model version 3 (CCSM3) as well as in other coupled climate models. This decadal peak has higher energy than is found in nature, almost twice as large in some cases. While previous analyses have concentrated on the mechanisms for such decadal variability in coupled models, an analysis of the causes of excessive SST response to changes in wind stress has been missing. Here, a detailed comparison of the relationships between interannual changes in SST and sea surface height (SSH) as a proxy for geostrophic surface currents in the region in both CCSM3 and observations, and how these relationships depend on the mean ocean circulation, temperature, and salinity, is made. We use observationally based climatological temperature and salinity fields as well as satellite-based SSH and SST fields for comparison. The primary cause for the excessive SST variability is the coincidence of the mean KE with the region of largest SST gradients in the model. In observations, these two regions are separated by almost 500 km. In addition, the too shallow surface oceanic mixed layer in March north of the KE in the subarctic Pacific contributes to the biases. These biases are not unique to CCSM3 and suggest that mean biases in current, temperature, and salinity structures in separated western boundary current regions can exert a large influence on the size of modeled decadal SST variability.

1. Introduction

Observations of a shift in the climate of the North Pacific Ocean around 1976–77 and the link to large-scale patterns in sea surface temperature (SST; Mantua et al. 1997) have lead to a search for potential sources of decadal variability in the ocean–atmosphere system in the North Pacific sector. Observations show two modes of variability in SST in the Pacific Ocean (Deser and Blackmon 1995), the first with a large expression in the tropics and a maximum of a different sign in the central Pacific, which is highly correlated with the El Niño–Southern Oscillation (ENSO). The second mode is independent of ENSO and is focused in the western North Pacific with a maximum along the Kuroshio Extension (KE). In addition, studies have shown that the SST and transport in the KE can be predicted by knowledge of the wind stress curl in the central North Pacific with about a 2–5-yr time lag (Schneider and Miller 2001; Deser et al. 1999). The time scale for delay comes from the time it takes for a wind-forced oceanic first baroclinic Rossby wave to propagate from the central North Pacific to the western boundary (Seager et al. 2001).

Ocean–atmosphere coupled models consistently show decadal peaks in the spectrum of SST in the Kuroshio–Oyashio Extension (KOE), and this peak has been attributed to a coupled ocean–atmosphere mode of variability (Latif and Barnett 1996; Pierce et al. 2001; Wu et al. 2005; Kwon and Deser 2007). Latif and Barnett (1996) analyzed a 70-yr integration of a fully coupled model ECHO-1 and found that decadal variability can be attributed to an unstable ocean–atmosphere interaction between the subtropical gyre circulation and the Aleutian low. Warm SST anomalies in the KOE are generated by wind-forced Rossby waves driven by an anomalously

Corresponding author address: LuAnne Thompson, Box 355351, School of Oceanography, University of Washington, Seattle, WA 98195.
E-mail: luanne@u.washington.edu

DOI: 10.1175/2010JCLI3402.1

strong Aleutian low and increased warm water advection. The atmospheric response to positive SST anomalies then weakens the Aleutian low, initiating the opposite phase of the oscillation. Pierce et al. (2001) examined decadal variability in the North Pacific in ECHO-2, an updated version of ECHO-1, and an integration of the Climate System Model version 1. They show that ocean dynamics within the North Pacific are necessary for the statistically significant decadal spectral peak of the KOE SST anomaly. While they found differences with Latif and Barnett (1996) in the dominant oceanic processes at work, they concluded that a coupled ocean–atmosphere mode was important in controlling decadal SST variability. Schneider et al. (2002), who also examined ECHO-2, concluded that the decadal time scale of the KOE variability results from the integration along Rossby waves trajectories of stochastic atmospheric forcing. They suggest a positive feedback such that anomalies of wind stress curl over the western North Pacific forced locally by KOE anomalies reinforces those anomalies. However, they found no negative feedback that would close the loop to create a true coupled mode of variability. In addition, they conclude the atmospheric response to the SST anomalies is primarily local. Kwon and Deser (2007) examine a 650-yr segment of the Community Climate System Model version 2 (CCSM2) control simulation. They too find that KOE SST exhibits significant peaks at 16 and 40 yr. They concluded that this mode of variability is a coupled mode with weak ocean-to-atmosphere feedback.

Despite the disparity of the interpretation of decadal variability in different coupled model analyses, the more recent work does agree on some key points (e.g., Pierce et al. 2001; Kwon and Deser 2007). First, the KOE SST anomalies result primarily from a meridional shift of the KE rather than from the advection of anomalously warm water by the current. This is supported by the observations and also ''ocean-only'' model studies (Seager et al. 2001; Nakamura and Kazmin 2003; Nonaka et al. 2006; Qiu et al. 2007). Second, the amplitude of decadal-to-interdecadal variability is larger than is found in observations estimates, as also discussed by Pierce et al. (2001, their Fig. 8). They show that the maximum spectral density at a frequency of 20 yr for the model is about 20% larger than in nature, with the region of local maximum located farther to the west, and that the region with large spectral density has a footprint that is about 50% larger in both the meridional and zonal extent than is seen in observations. In a different model Climate System Model, version 2.1 (CSM2.1) [Geophysical Fluid Dynamics Laboratory (GFDL) Climate Model version 2.1], Knutson et al. (2006) find the standard deviation of interannual SST in the KOE to have maximum amplitude of about 0.6°C in an analysis of observations, while the model has a maximum amplitude of 1.5°C. Alexander et al. (2006) also show pronounced variability in a control simulation of the Community Climate System Model version 3 (CCSM3) of SST in the KOE that we explore in detail in this paper.

While this overexpression of decadal KOE SST variability is a common feature among many state-of-the-art coupled climate models, the excessive SST variability in the KOE has not been the focus of previous studies. We focus on the cause of the excessive signal here. In ocean-only hindcast simulations driven by the observed wind stress curl forcing and run at low resolution, a similar enhancement of decadal SST variability as that seen in the coupled models is also apparent. For instance, Seager et al. (2001) find that the SST difference between two 8-yr periods before and after the 1976 climate shift is larger than in observations. There are questions about whether the ocean is adequately sampled to give a realistic representation of the true variability in observational analyses; however, we argue below, using new high-resolution datasets and an analysis of a CCSM3 simulation, that low-resolution models consistently overrepresent the SST variability in this region.

While the large-scale adjustment of the gyre circulation to changes in wind stress curl has been successfully modeled both in full ocean general circulation models (Seager et al. 2001) and in simplified models (Qiu 2003), the western boundary current systems remain difficult to model, particularly when the models do not resolve the mesoscale eddy field. Most coupled climate models are run with a low-resolution (~1°) ocean component with low Reynolds' number. The lack of eddy mixing and an eddy-driven recirculation gyre results in large biases in the KE and Oyashio Extension (OE) system. The implication of the mean biases in the ocean on the simulated excessive decadal SST variability in KOE is the particular focus of this study.

In the western North Pacific, the subtropical gyre returns to the interior via the KE, located near 34°N in nature, whereas the OE closes the subpolar gyre circulation by separating from the coast near 40°N. Between the two systems lies the mixed-water region, where the North Pacific Intermediate Water (NPIW) that originates in the Okhotsk Sea is modified (Talley 1997). At high enough ocean resolution, these current systems can be well represented (for instance, see discussion of the 10-km simulation by Nonaka et al. 2006). However, at noneddy-resolving resolution, two distinct currents do not exist. Instead, the diffuse nature of the circulation results in only one western boundary current extension, with latitude at about that of the OE found in high-resolution simulations and in nature. Thus, in most climate models, the two currents are treated as one and named the KOE.

The mean ocean biases near the KOE manifest in temperature, salinity, mixed layer depth (MLD), and water mass distribution. Large and Danabasoglu (2006) show a large warm SST bias occurs in the KOE in the CCSM3. Thompson and Cheng (2008) compare a fully coupled model against the ocean-only model forced with atmosphere without year-to-year variability and show that biases in SST, circulation, and vertical structure in the ocean component of the coupled model originated in the ocean model for the most part and are not forced by errors in the atmospheric component. In addition, the subarctic North Pacific tends to be too fresh at the surface (Large and Danabasoglu 2006). They did not focus on the reasons for why the surface subarctic Pacific is too fresh, but as we show below, this can be attributed to the too shallow NPIW in the model. Gent et al. (2009) shows an improvement in SST in the KE when the atmospheric model resolution is increased while the ocean model resolution remains the same, although cold and fresh biases in the OE and subarctic Pacific increase with the increased atmospheric resolution.

To explore why the excessive KOE SST variability exists in the models, we compare the SST variability with a center of action in the KOE from a 100-yr CCSM3 control simulation with that of observations. To determine the source of the bias, we first review the representation of the mean oceanic circulation of the region in CCSM3, with comparisons to both an ocean-only simulation as well as observations. Next, we examine the amplitude of the decadal variability in KOE SST, including relationships with the other variables via correlations, EOFs, and canonical correlations between sea surface height (SSH) and SST to identify differences from observationally derived relationships. We finally examine a diagnostic relationship that explains the amplitude of the decadal KOE SST variability based on the mean ocean state and the movement of the KOE, although this relationship does not hold for the observations. In an appendix, we briefly discuss internal modes of oceanic variability in an ocean-only version of the model and show that the amplitude of such variability in this model is much smaller than the signal in the coupled model. We follow with a summary of how mean biases in the representation of both the currents and the temperature and salinity in the KOE region lead to excessive SST variability.

2. Models and data

CCSM3 is a well-documented state-of-the-art coupled climate model (see the June 2006 issue of the *Journal of Climate* for a complete analysis of the model construction and performance; Collins et al. 2006). Here, we only give a brief introduction of the runs we analyzed. The atmospheric component in the coupled model uses a T85 spectral truncation (equivalent to $1.4° \times 1.4°$ grid spacing) and 26 vertical levels. The radiative forcing is fixed at 1990 levels for anthropogenic greenhouse gases, ozone, and aerosols. The ocean and sea ice models share the same horizontal grid, with approximately 1° longitudinal resolution and variable latitudinal resolution that is finest near the equator at 0.27° and coarsest in the far northwestern Pacific (~0.6°). The ocean component is described in detail in Gent and Danabasoglu (2004). The Gent and McWilliams (1990) parameterization is used that mixes along isopycnals with a Laplacian operator with a diffusion value of 600 $m^2 s^{-1}$ and there is an additional eddy-induced transport of tracers. There are 40 levels vertically in the ocean model. The model output used in this study is from years 500–599 of the 700-yr control simulations. All model outputs were saved as monthly averages during the run. We term this run CPL, which stands for coupled.

To understand to what extent mean biases in the coupled model stem from biases due to the internal ocean model physics versus those from biases in the surface forcing due to atmosphere–ocean coupling, we also examine simulations by the stand-alone ocean component of CCSM3, the Parallel Ocean Program (POP) model, driven by prescribed atmospheric forcing without any year-to-year variability. The forcing is based on the observation-based Common Ocean-Ice Reference Experiments (CORE, available online at http://data1.gfdl.noaa.gov/nomads/forms/mom4/CORE.html; Large and Yeager 2004), constructed as a repeated annual cycle. The atmospheric forcing is applied via bulk aerodynamic formulae for the turbulent fluxes using model SST, and virtual salt flux is used for forcing the sea surface salinity. No extra surface restoring is used for SST, while sea surface salinity (SSS) has a restoring flux with time scale of 91 days. We used model years 400–500 for this analysis. We term this run OCN, which stands for ocean only.

We also briefly discuss 70 yr of high-resolution (0.1°) simulation using POP forced by the same repeated annual forcing as in OCN (Maltrud et al. 2010) to see to what extent the excessive SST variability can be simply attributed to the low ocean resolution of CPL or OCN.

For the observational analysis, we use two SST products: the National Oceanic and Atmospheric Administration (NOAA) high-resolution ($0.25° \times 0.25°$) SST version 2 [an Advanced Very High Resolution Radiometer (AVHRR)-only product] from 1982 to 2008 (available online at http://www.ncdc.noaa.gov/oa/climate/research/sst/oi-daily.php; Reynolds et al. 2007) and the lower-resolution Extended Reconstruction SST version 3 (ERSST, available online at http://www.ncdc.noaa.gov/oa/climate/research/sst/ersstv3.php; Smith et al. 2008)

2° data from 1909 to 2008. We also use a merged SSH product from multiple radar altimeters [including TOPEX/Poseidon, *Jason-1*, the European Remote Sensing Satellite (ERS), and *Envisat*] from the Archiving, Validation, and Interpretation of Satellite Oceanographic data (AVISO, available online at http://www.aviso.oceanobs.com; Ducet et al. 2000), supplemented by a mean sea surface derived from gravity and ocean in situ data (Maximenko and Niiler 2004). SSH maps are available weekly, beginning in November 1992. The SSH field is used to examine the fidelity of the location and variability of the KOE current system in the model simulations. For all of the analyses, we use yearly averaged fields as we are focused on interannual-to-decadal variability.

In addition, model-simulated upper-ocean temperature and density as well as MLD are compared against observations. The MLD for both models and observations is defined based on a potential density change from the surface of 0.125 kg m^{-3}. Model MLDs were compared against those derived from observational data in the *World Ocean Atlas 2001* (WOA01; Conkright et al. 2002).

3. Representation of the mean circulation and water properties in the KOE

The structure of the wind-driven circulation in the North Pacific in the broadest sense is well represented by climate models, with the location and structure of both the subtropical and subpolar gyres qualitatively correct, once biases in wind stress are taken into account [see Thompson and Cheng (2008) for further discussion of wind stress–forced ocean biases in CCSM3.0]. Biases in mean surface heat and freshwater fluxes for the most part occur because of biases in ocean circulation. They do not originate in the atmospheric component of the model (Thompson and Cheng 2008). However, when one looks in more detail at the western boundary current extension region, larger mean biases become apparent as discussed in the introduction. Large variability in SST generally occurs in regions of high horizontal SST gradient and large surface currents, with large surface current corresponding to regions of large SSH gradients. In the KOE, there are local maximum in both SST gradients and surface currents in both the model and observations. The magnitude of the gradient in SSH in the model has a distinct maximum near the western boundary extending into the interior (Fig. 1a), representing the location of the KOE in the model. The meridional extent of interior maximum is much larger in the model, and its center is located near 38°N as opposed to about 34°N in the observations (Fig. 1c). There is a hint of a secondary interior maximum near 38°N in the observations, likely representing the location of the OE that is distinct from the KE. OCN also shows a similar SSH gradient as CPL (not shown), indicating that the KOE is represented in a similar fashion in CPL and OCN and that the mean biases in the KOE primarily originate in ocean model biases, not in atmospheric biases (see also Thompson and Cheng 2008). Thus, the KOE in the model is one diffuse broad current with no distinct OE in the model. The weaker SSH gradient in the model KOE compared to the observed KE also indicates a weaker simulated current. The consequences of this bias are numerous, including SST in both OCN and CPL being too warm near the coast and too cold downstream (Fig. 5 of Thompson and Cheng 2008; also Large and Danabasoglu 2006). In addition, the SST gradient in the model is at a maximum near 40°N (Fig. 1b), adjacent to the KOE to the north. In observations, the SST gradient is maximum in the OE near 40°N (Fig. 1d), with a local maximum at the separation of KE from Japan of the KE near 36°N. The SSH gradient maximum along the KE is separated by 5° of latitude or more to the south from the maximum SST gradient.

The current, temperature, and salinity structure also causes biases in winter MLD with two features distinctly different from that found in observations (Fig. 2). In nature, the MLD has a local maximum south of the KE front, which coincides with the formation of subtropical mode water, and deeper March mixed layers in the mixed-water region where central mode water forms near 42°N (Fig. 2b; Hanawa and Talley 2001). However, in the model, there is one large region of deep mixed layers that coincides with the center of the KOE (Fig. 2a). To the north of the KOE around 44°N, there is a region of relatively shallow MLDs that does not exist in nature (Fig. 2b). The source of the shallow MLD near 44°N in CPL is linked to the structure of the subarctic gyre and is associated with a large freshwater bias at the surface. As noted in Thompson and Cheng (2008), the NPIW in both CPL and OCN as well as other low-resolution ocean models is poorly represented. In nature, this water mass is believed to originate in the Okhotsk Sea (Talley 1993). That water is then transformed as it exits through the passages between the Kuril Islands and then reaches the mixed-water region between the KE and OE (Talley 1997). However, in low-resolution models, the NPIW tends to form near the surface just to the north of the KOE (Kobayashi 1999, 2000). A temperature section at 150°E shows that, in both the model and observations, the NPIW is characterized by a temperature minimum near the western boundary (Fig. 3). It is, however, much shallower in CPL than in nature, with the water too fresh even at the surface (not shown). The temperature minimum is compensated by a shallower salinity minimum in CPL that results in an

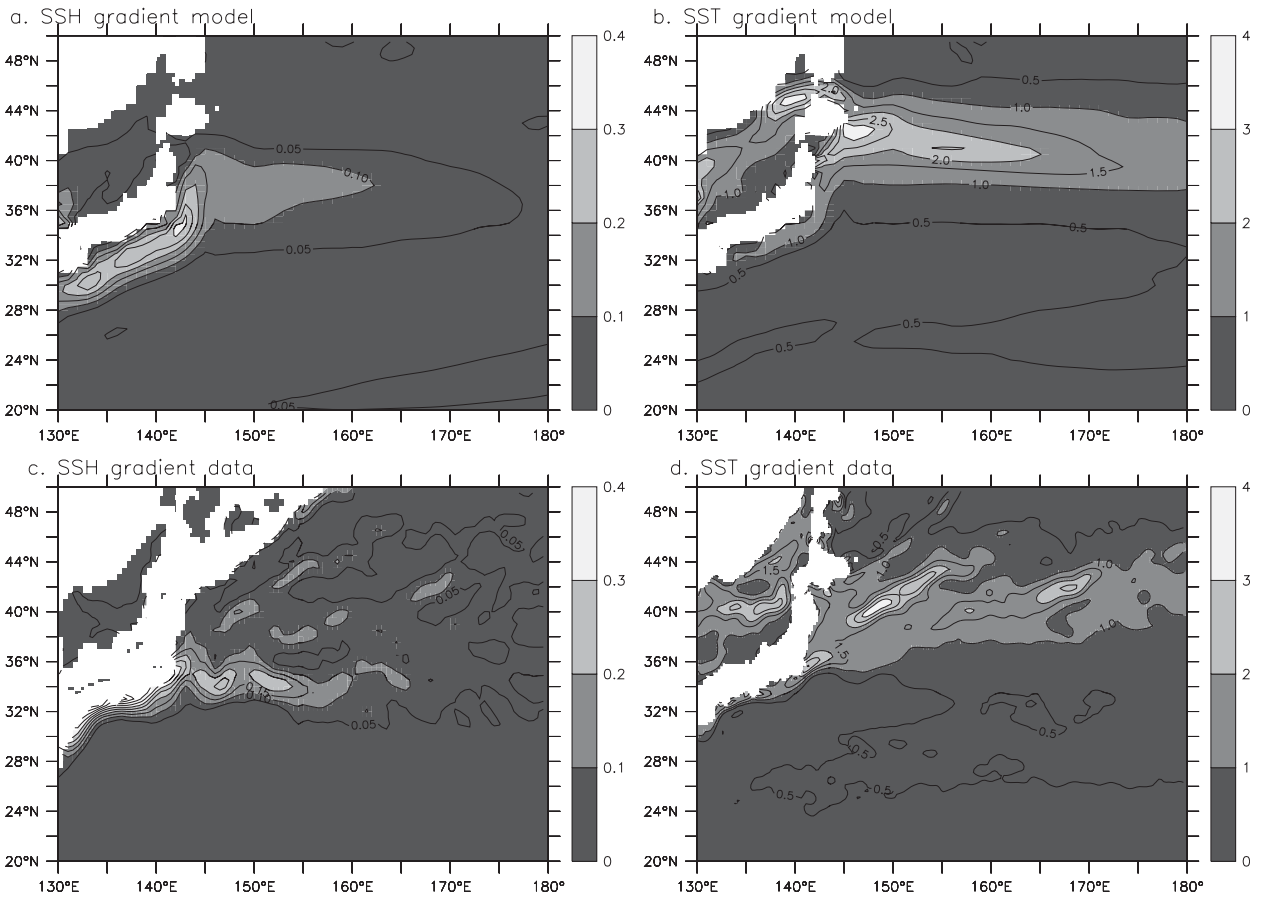

FIG. 1. Mean strength of the SSH and SST gradients: (a) SSH gradient for CPL [m (100 km)$^{-1}$], (b) mean SST gradient for CPL [°C (100 km)$^{-1}$], (c) mean SSH gradient from Maximenko and Niiler (2004) [m (100km)$^{-1}$], and (d) mean SST gradient from NOAA 0.25°SST [°C (100 km)$^{-1}$].

excessively stratified water column (not shown). As a consequence, the shallow NPIW creates a region of strong stratification just north of the KOE, and this keeps the winter MLD shallow in the model (see the density contours in Fig. 3).

4. Characterization of interannual variability in SST in the KOE in observation and models

While the simulated mean oceanic structure has locally large biases, it could be argued that these biases play an insignificant role in controlling the mean climate of the region in the coupled model. Here, we evaluate how well the variability is represented in CPL using available observations of both SST and SSH. We do this by constructing both EOFs and area-averaged metrics.

a. SST variability

As discussed in the introduction, CPL has maximum standard deviation in SST that is at least twice as big as that seen in observations (Figs. 4b and 4d) when compared over the 27-yr-long NOAA 0.25°SST. To see if our analysis is biased by using annual means, we also examined wintertime SST anomalies since the SST anomaly in winter is higher than that in summer. We find that the maximum standard deviation of CPL SST is over 2.6°C for winter (December–March) and the observational counterpart is over 1.4°C while for the annual mean they are 1.8°C for CPL and 1.0°C for the observation, indicating that, if anything, the examination of annual means underestimates the SST variability difference between the observations and CPL.

To determine if the shorter observational time series biases the results, the standard deviation of SST for each 27-yr segment of the 100-yr ERSST dataset (Smith et al. 2008) is calculated, and the same is done for the model SST. Since the maximum variance is located in a different location in model and observations, we used different domains for averaging. For the model, we used 40°–45°N, 144°–164°E, and for the data we used 35°–40°N,

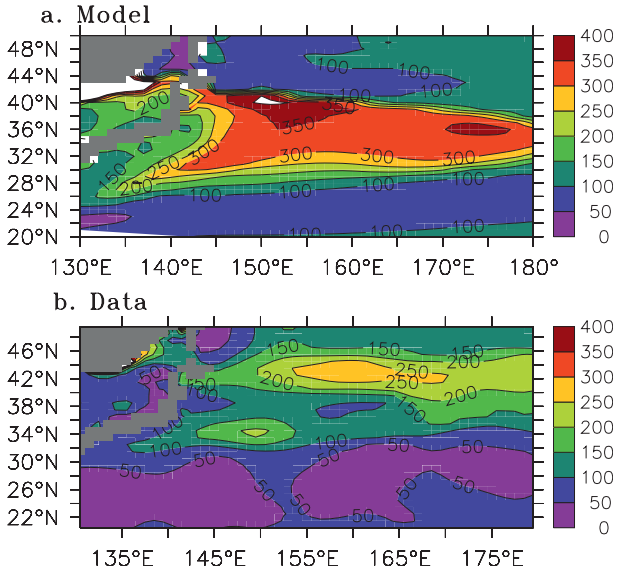

FIG. 2. March mixed layer depth (m) from (a) CPL and (b) derived from WOA2001.

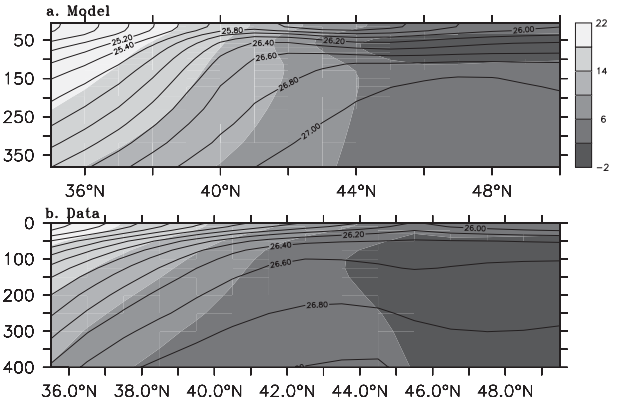

FIG. 3. Annually averaged potential temperature (°C; shading) and potential density minus 1000 kg m^{-3} (contours) section at 150°E from (a) CPL and (b) WOA2001.

137°–162°E. Since we are spatially averaging the SST first, before the standard deviation is calculated, the results should be consistent among the different datasets with differing spatial resolutions. The maximum standard deviation over the longer observational times series is always smaller than the standard deviation from equivalent length model time series (Table 1).

In addition, standard deviations of SST for 27-yr segments from the 70-yr-long 0.1° high-resolution POP simulation have been calculated in two different ways for comparison. First, the native resolution of the model (=0.1°) was used. The SST standard deviations are greater than the ones from either of the observations but still smaller than those from CPL (Table 1). The result suggests that the excessive SST variability in CPL cannot be simply attributed to the low ocean resolution alone, but it should be understood in terms of biases resulting from the low resolution. Then, we subsample the high-resolution SST in 1° resolution to examine the influence of resolution in observational datasets. The subsampled SST exhibits slightly smaller standard deviations than the ones calculated from the full resolution, indicating that the limited resolution of the observations could result in underestimation of the SST variability but only by a small amount.

Averaged over the above respective regions of maximum SST variability for the model and data, the spectrum of variability of spatially averaged SST shows that not only is the amplitude higher on interannual-to-decadal time scales, but the decadal peak at around 15–20 yr is significant, whereas in the observations a distinct decadal peak is absent (Fig. 5). Note that for the spectral analysis the annual mean 2° ERSST from 1909 to 2008 is used for the observed SST since the high-resolution SST is too short to resolve decadal or longer periods.

Finally, the mean SST in the region of maximum SSH (or surface current) variability is different in the model and observations. For the model, the mean SST averaged over the KOE region is 10°C, whereas in the observations the mean temperature of the region with maximum SST variability is 18°C.

b. SSH and current variability

One possibility for the larger SST variability in the KOE in the model is that the meridional movement of the KOE front in response to changes in wind is excessive in the model. To quantify the meridional movement of the KE in data and the KOE in the model, we define the location of the KE and KOE in data and models, respectively, by their maximum surface geostrophic currents based on SSH. For the model, we defined the location as the latitude with maximum zonal geostrophic flow at each longitude, which is equivalent to the location of the maximum in the meridional gradient of the SSH. For the observations, we defined the location by fitting the SSH to an error function using the method of Kelly (1991) and Kelly et al. (2007). The two different definitions are required because the current has very different meridional structure in the model and the observations, with it being much more localized in observations. Averaged between 144°E and 180°, the KOE in the model is located near 39°N, while the KE in observations is located near 34°N as seen also by the differing locations of the maximum in mean SSH gradient in Figs. 1a and 1c. The standard deviation of the zonally averaged location between 144°E and 180° for the model is 0.65°, while that of

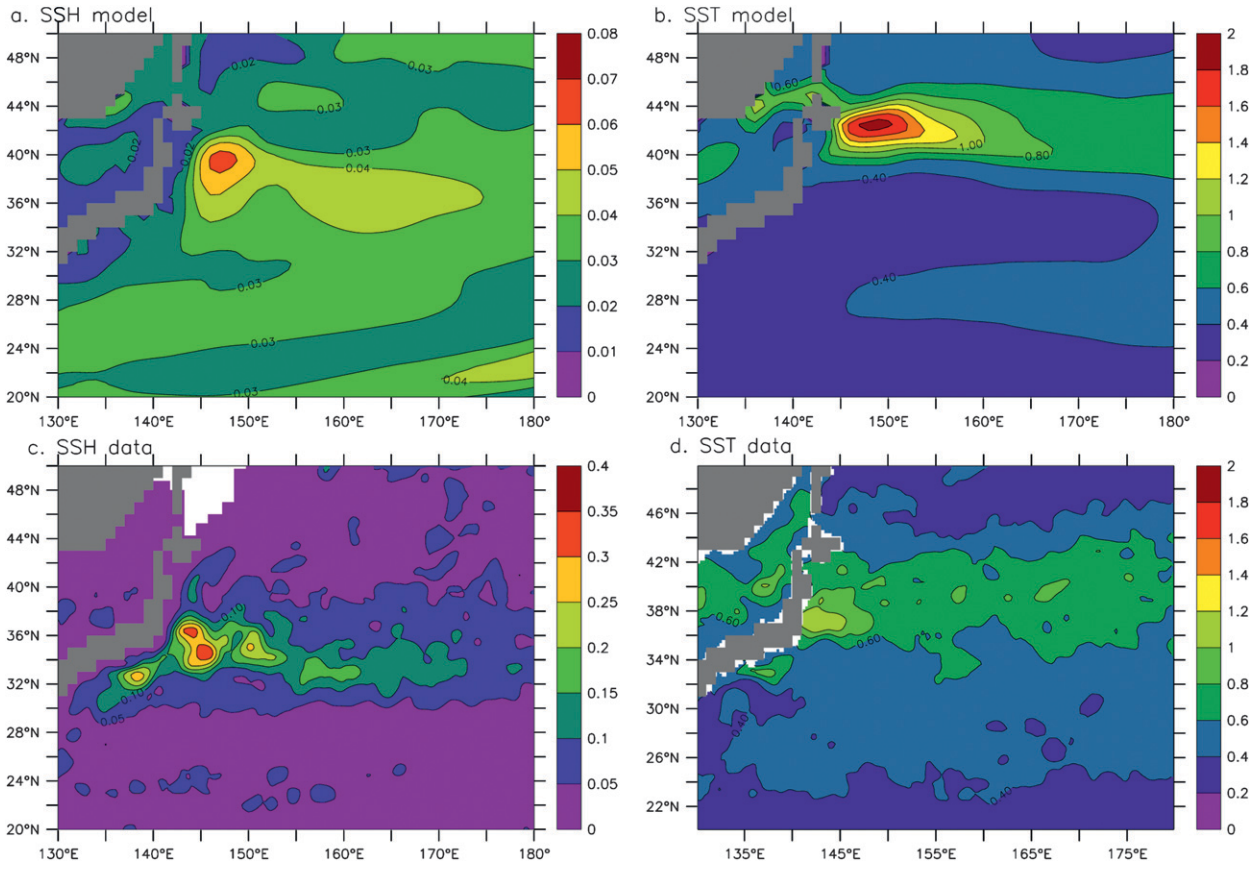

FIG. 4. Standard deviation of annually averaged SSH (m) and SST (°C). (a) SSH from CPL, (b) SST from CPL, (c) SSH from AVISO, and (d) SST from NOAA 0.25°SST (°C) are shown. Notice the different scaling for SSH between (a) and (c).

the observational locations is 0.45°. Keeping in mind that the observational record is much shorter than the model record, the standard deviation in the location of the front in the model is about 50% higher than found in the observations, suggesting that the model current may be overly responsive to changes in wind. However, the result may be limited by the model resolution and the statistical significance may not be robust. Therefore, overly responsive KOE current to changes in wind alone cannot fully explain the excessive SST variability in the KOE.

c. *The relationship between SST and currents*

We next examine the relationship between SST variability and the current variability based on regressions of SST onto the time series of the zonally averaged locations of the observed KE and modeled KOE for observations and CPL, respectively (Fig. 6). In CPL, the maximum SST response to changes in the KOE is coincident with the location of the maximum SSH variance (cf. Fig. 6a with Fig. 4a). The region of SST response larger than 0.6°C in the model is localized near 40°N, 155°E. The zonal extent of this feature is at least 30° of longitude. In contrast, in the observations there is a localized maximum in SST response coincident with the KE SSH variability (cf. Fig. 6b with Fig. 4c) at 34°N. The observed SST response in the KE has much smaller zonal extent and is less spatially coherent than what is seen in the model response to changes in the KOE. There is also another local maximum

TABLE 1. Mean, maximum, and minimum standard deviation for each 27-yr segment of each time series of SST (°C) averaged over 35°–40°N, 137°–162°E for the observational time series and the high-resolution model and over 40°–45°N, 144°–164°E for CPL.

SST source	Mean std dev	Max std dev	Min std dev
ERSST (100 yr)	0.52	0.64	0.41
0.25°SST (27 yr)	0.57	0.57	0.57
High-resolution model at full resolution	0.77	0.77	0.76
High-resolution model at 1° subsample	0.71	0.73	0.66
CPL (100 yr)	0.95	1.18	0.70

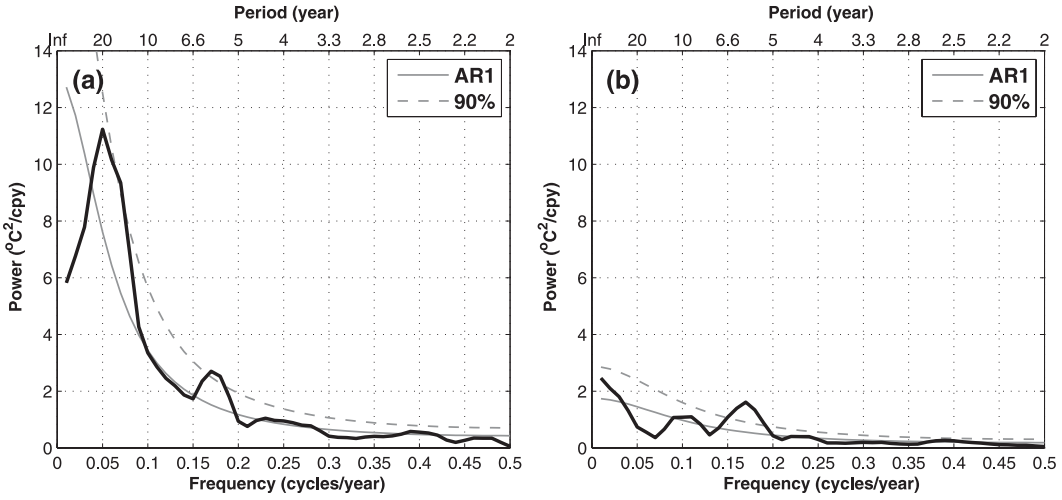

FIG. 5. Spectrum of SST from (a) CPL model and (b) ERSST observations (1909–2008), averaged over 40°–45°N, 144°–164°E for the model and 35°–40°N, 137°–162°E for the observation. Note that the lengths of time series are 100 yr for both. The best-fit first-order autoregressive model (AR1) spectrum and associated 90% significant level are plotted with solid and dashed gray lines, respectively, based on the 1-yr-lag autocorrelations of the respective SST time series.

in the observations near 40°N coinciding with the location of the OE. This suggests that in nature there is localized direct response to changes in the KE location and coherent but weaker changes along the OE. In addition, there are coherent changes in the central Pacific between 155° and 175°E.

In the model, the maximum response to changes in the KOE is located just to the south of the maximum standard deviation to the interannual SST anomaly (cf. Fig. 4b to Fig. 6a), indicating that changes in the KOE are likely closely linked to the maximum in the SST interannual variance. However, in the observations the maximum response to changes in the KE is located coincident to the SSH variability maximum (cf. Fig. 4c to Fig. 6b) but not the SST variance maximum. The observed interannual SST variance maximum is located near the secondary maximum near the OE at 40°N (cf. Fig. 4d to Fig. 6b), and the SST variance maximum is not coincident with the SSH variance maximum (cf. Fig. 4c to Fig. 4d).

To further examine the relationship between the SSH and SST in model and observations, we estimated the canonical correlations between the SSH and SST using the method of Kelly et al. (1996). First, the EOFs are calculated separately for the two fields, and the first seven EOFs are retained, with the seventh EOFs explaining about 10% of the variance of the first EOF for both fields. This allows the analysis to be made on spatially smoothed fields. The first seven EOFs as a whole retain 71% and 62% of total variance for SST and SSH, respectively, in the model. The correlated patterns are then found and reconstructed to give the canonical correlations. Finally, the patterns are scaled by the standard deviation of the associated time series (Fig. 7). The second SST EOF over the full 27-yr observational record was different than that over the 15-yr record overlapping with the satellite SSH data, so we concentrated our analysis on the leading SST EOF pattern that is robust to changing time-series length. The SSH anomalies are much smaller in the model than in the observations, however, the corresponding SST anomalies are larger in the model than in observations, consistent with the results seen in Fig. 4. Both the model's and observation's first mode show a local maximum in both SSH and SST in the central North Pacific. This pattern likely reflects the oceanic response to changes in the large-scale wind field and a local response to a PDO-like forcing (Alexander et al. 2002).

In the mean, south of the KOE–KE the mean SSH is high while to the north it is low. A northward shift of the KOE–KE would be represented as a high SSH in the canonical correlation located just to the north of the mean SSH gradient. In the canonical correlation, there is a large coherent signal in the model between 40° and 45°N with SST amplitude over 2°C (Fig. 7b). This is related to a local maximum in SSH near 40°N, 150°E, just north of the mean location of the KOE (Fig. 7a). This suggests that the SST anomaly can be linked to a northward shift of the KOE. The observations show a similar pattern that is much smaller in spatial extent and magnitude with SST high just north of 35°N (Fig. 7d). However, unlike in the model, the SST and SSH anomalies are

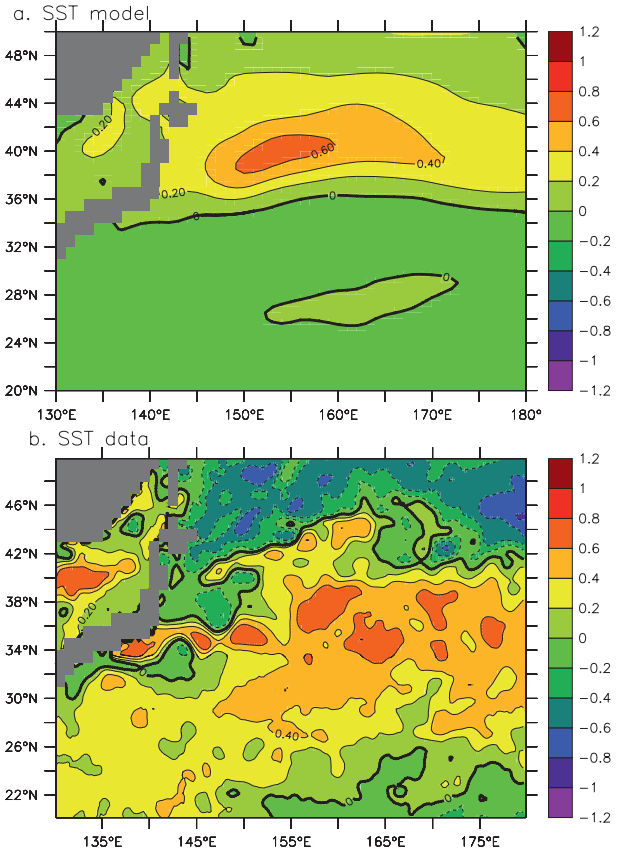

FIG. 6. Regression of annually averaged SST onto zonally averaged KOE–KE path. (a) CPL with KOE path zonally averaged between 144.5° and 164.5°E and (b) NOAA 0.25°SST with KE path zonally averaged between 141.5° and 164°E are shown.

coincident in space, suggesting a subtle difference in the processes that relate changes in the KOE–KE to changes in SST between the observations and the model. The region of high SSH and SST is coincident with the local minimum in MLD in observations (Fig. 2b). If the analysis is done over only the KOE region, the first canonical modes are very similar to those shown in Fig. 7. The local maximum in SST for the first canonical mode is very similar for both observations and model to their respective standard deviation (Fig. 4).

Changes in the KOE results in SST variability, and the KOE changes are driven by earlier wind stress changes in the central North Pacific as was confirmed by the earlier work of Kwon and Deser (2007). Schneider and Miller (2001) found that central North Pacific wind stress curl leads wintertime Kuroshio SST by 2–3 yr when they modeled the Kuroshio SST by a simple Rossby wave model. The SST in the KOE, the location of the KOE, and the first canonical mode are also all highly correlated in both the observations and in the model.

d. Decadal peak as an internal oceanic mode of variability

It has been suggested that decadal climate variability may be due to internal modes of variability that exist in an uncoupled ocean forced by climatological surface forcing without any year-to-year variability. We find that for OCN, on decadal time scales, the internal mode of variability has extremely small amplitude (on the order of 0.001°C temperature anomaly). While its spatial pattern is similar to that of the model first canonical mode described above, we conclude that it is not likely to be the source for the decadal variability at least in this low-resolution model (see appendix).

5. Controls of the amplitude of the KOE SST variability

Based on the coherent SST signal in the KOE in the model, and its correlation to path changes of the KOE front, a diagnostic relationship can be derived between the size of the SST anomaly, the mean SST gradient, and the distance that the KOE moves in a year away from its mean position in response to changes in the wind stress. In CPL, averaged between 144° and 164°E, the model SST gradient is broad with its maximum located near 40°N while the maximum mean SSH gradient is located near 38°N (Fig. 8c). In contrast, the observationally determined maximum SST gradient is located near 41°N and has a narrower latitude range, whereas the maximum gradient in SSH occurs at 34°N (Fig. 8d), well separated from the maximum SST gradient. In both cases, the maximum standard deviation SSH is located near the respective maxima in the SSH gradient (Figs. 8a and 8b), with a much smaller magnitude seen in the model.

An approximate scaling for the size of the meridional displacement of the currents as a function of latitude is

$$(\overline{d'^2})^{1/2} \approx \frac{(\overline{\eta'^2})^{1/2}}{d\overline{\eta}/dy}. \qquad (1)$$

Here, d is the displacement of the SSH contours, y is the meridional coordinate, and η is the sea surface height. The overbar indicates an average over the time series of interest, while the prime indicates the deviation of the annual mean from the long-term average. The SSH displacement calculated from (1) for the model has a maximum near 42°N, whereas in the observations there are two local maximum: one near the KE at 36.5°N and the other near the OE at 42°N. These correspond well to the locations found in Fig. 4 for the maxima in SSH variance. Since the maximum SST anomalies do not

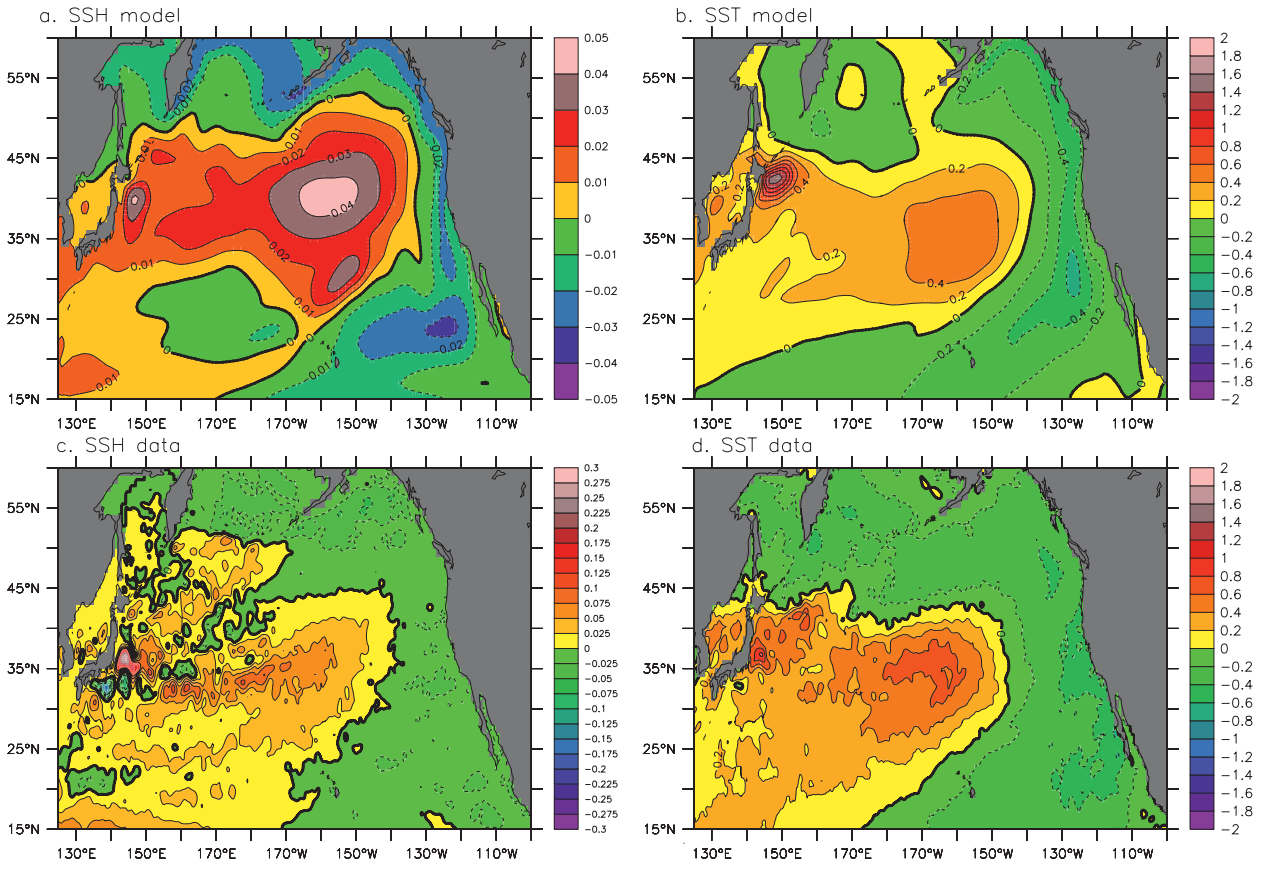

FIG. 7. First canonical mode of SST (°C) and SSH (m) scaled by the standard deviation of the respective time series. (a) CPL SH, (b) CPL SST, (c) observational SSH, and (d) observational SST are shown.

necessarily come from regions of the maximum geostrophic current, we use (1) as a measure of displacement throughout the entire KOE–KE system.

Based on (1), a diagnostic for the amplitude of the SST variability may then be written as

$$(\overline{T'^2})^{1/2} \approx \frac{(\overline{\eta'^2})^{1/2}}{d\overline{\eta}/dy}\frac{d\overline{T}}{dy}. \qquad (2)$$

Here, T is the SST, and the standard deviation of SST should be given by standard deviation of the displacement of the KOE (or KE) and the gradient in mean SST. This estimate reproduces the CPL SST variance remarkably well (Fig. 8e). The estimate has an RMS error of 0.14°C when evaluated between 38° and 46°N. This indicates, as the other authors have noted, that the shifts in the KOE against the mean SST gradient produce variability in the SST in the model. In addition, the SST response is enhanced further than that given by (2) just north of 46°N where the MLD abruptly thins.

However, the diagnostic relationship in (2) does not work well for the observations, with the predictions from (2) having 0.81°C RMS error with respect to the observed SST variability. In the observations, not only are the maximum gradients in the mean SST and SSH separated by 500 km, the processes that control the interannual SST are more complex than suggested by (2), such as the KE and OE interaction with the local minimum MLD in the mixed-water region (Fig. 8b versus Fig. 8a). The one place where (2) works well is at 38°N, coincident with the local minimum in MLD. While previous authors have shown that SST changes in the KE can be directly linked to displacements of the KE (e.g., Qiu 2000), the maximum interannual variance in SST is located well to the north of the KE with its peak near 38°N almost exactly between the KE and the OE in the local minimum in MLD.

For both the model and the observations, the local minimum in MLD appears to be linked to a maximum in standard deviations in interannual SST anomalies. We surmise that it is at the region of local minimum in MLD that the SST is most responsive to changes in currents.

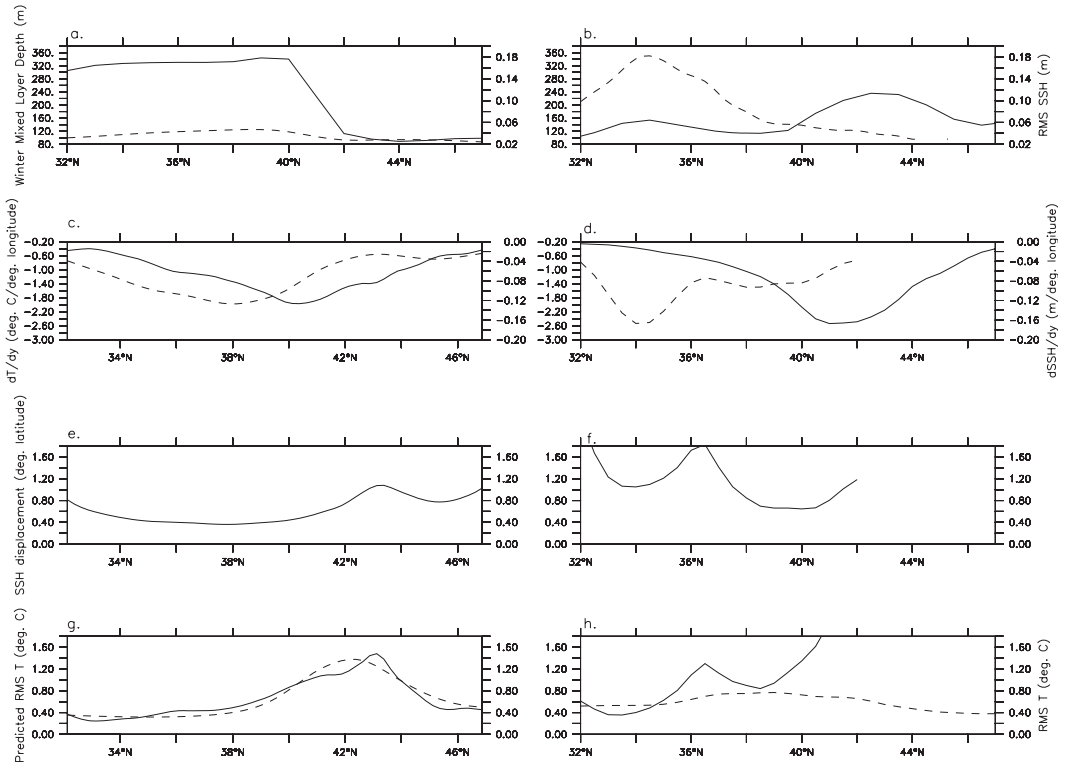

FIG. 8. Zonally averaged quantities between 144° and 164°E for (left) CPL and (right) observations. (a),(b) MLD (m, solid line, lhs scale) and standard deviation of SSH (m, dashed line, and rhs scale), (c),(d) SST gradient (solid line; lhs scale in degrees Celsius per degree of latitude) and SSH gradient (dashed line; rhs scale in meters per degree of latitude), (e),(f) predicted current displacement from (2) (degrees of latitude), and (g),(h) predicted SST from (2) (solid line) and standard deviation of SST (dashed line; °C).

6. Conclusions

While mean biases in the surface ocean in standard coupled ocean–atmosphere climate models have long been noted, we have shown here that these biases also have consequences for how the coupled system represents interannual-to-decadal variability in SST. Whether modeled decadal modes of variability in the midlatitude North Pacific are representative of a coupled ocean–atmosphere mode, or whether they are an accurate representation of modes of variability in nature has long been debated. Here, we show that interannual-to-decadal variability of SST in the KOE in coupled climate models is excessive, and that the excessive amplitude can be understood based on the structure of the mean ocean circulation and stratification biases in the climate models.

The sources of the errors in the mean model ocean are not simple. Not only do they come from the poor representation of the KE and OE in the noneddy-resolving ocean component, they also depend on the poor representation of processes that create a too fresh and shallow NPIW in the subarctic gyre and the consequent misrepresentation of MLD. We did find that the SST in the KOE can be realistically attributed to the meridional movement of the KOE front. However, because the location of the maximum meridional gradient in SST is just to the north of the center of the KOE in the model, the SST response is excessive. In the model, the SST can be easily predicted with knowledge of the meridional gradients in SST, SSH, and the SSH variance. However, the SST response in the observations is not easily estimated from these quantities. This scaling overestimates the SST response in both the OE and KE and does not predict a maximum in interannual SST variance between 38° and 40°N. Instead, the SST in observations is controlled by other processes such as the interaction of the KE–OE system with the mixed layer in the mixed-water region.

It is important to note that CCSM3 is not unique in its poor representation of the KOE. The diffuse front and lack of distinction between the OE and KE is typical of low-resolution climate models. In addition, the representation of the subarctic Pacific is similar to that in other models. Decadal modes of variability in coupled climate models have been described in other ocean

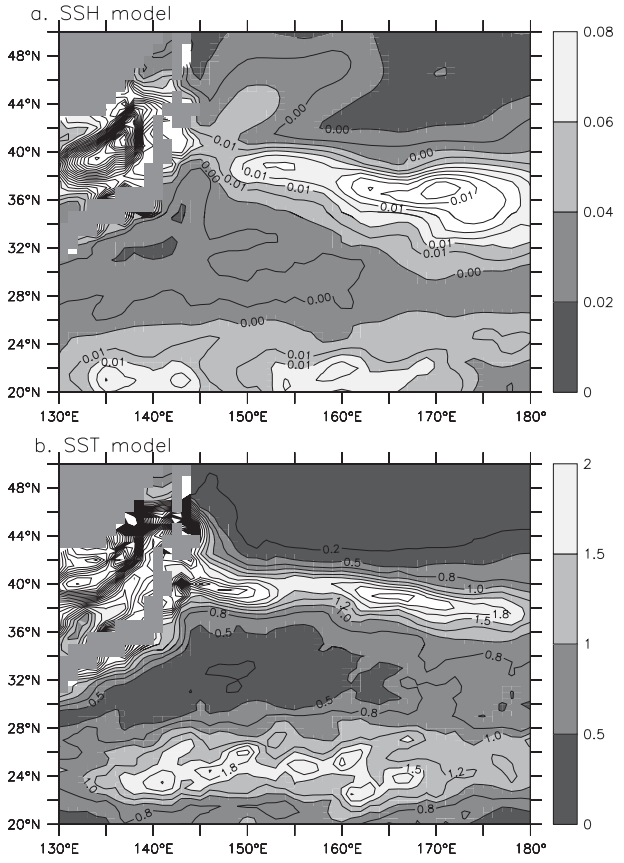

FIG. A1. Standard deviation of annually averaged SSH and SST from OCN. (a) SSH (10^{-3} m) and (b) SST (10^{-3} °C) are shown.

basins, Danabasoglu (2008) describes where a multidecadal mode of variability centered in the subpolar North Atlantic in CCSM3. He notes that the pattern and magnitude of the dominant SST variability are not realistic. He also notes that the regions of highest SST and SSS variability are roughly collocated to the location where the mean SST and SSS biases are the largest. The center of action is in the North Atlantic Current where there is a large mean SST bias owing to poor representation of the path of the current. As in the North Pacific, the North Atlantic biases may have their source in the subpolar side of the separated western boundary current, especially if we draw a parallel between the poor representation of the OE and the North Atlantic Current.

Acknowledgments. Support for L.T. was provided by the NASA sponsored Ocean Surface Topography Science Team, under Contract 1267196 with the University of Washington, administered by the Jet Propulsion Laboratory. Support for Y.-O. K. comes from the NOAA Office of Global Programs (grant to C. Deser and Y.-O. Kwon) and the WHOI Heyman fellowship. The AVISO altimeter products were produced by the CLS Space Oceanography Division as part of the Environment and Climate EU ENACT project (EVK2-CT2001-00117) and with support from CNES and can be obtained online from http://www.aviso.oceanobs.com. We also thank two anonymous reviewers for helping to significantly improving the manuscript.

APPENDIX

Ocean Internal Modes of Variability

Internal modes of variability often exist in the ocean component of climate models (e.g., see Primeau 2002). Dawe and Thompson (2005) argue that, in some cases, the internal mode of variability can be spurious because its existence depends on the presence of very long wave baroclinic instability. A 1° ocean model does not allow for the growth of the most unstable mode of the unstable jet, whose wavelength is about the distance between the grid boxes. Instead, there is a baroclinically unstable very long wave baroclinic instability of which the shortest wavelength is resolved by the model. The instability originates in the return flow of the subtropical gyre near 24°N, it then propagates and generates in the KOE. A similar mode of variability was also seen in a North Atlantic simulation (Hazeleger and Drijfhout 2000).

This mode of variability appears in OCN, although the amplitude of its expression in SSH and SST is extremely small (Fig. A1). The maximum SSH standard deviation is 0.000 12 m while the maximum SST standard deviation is 0.0023°C. The maximum in SST is located downstream in the KOE and is located near the maximum variability in SSH. Notice also the variability in the return flow of the subtropical gyre near 24°N. This is the genesis region of the internal mode as discussed by Dawe and Thompson (2005), where the potential vorticity structure is favorable to baroclinic instability. The first canonical correlation mode (not shown) shows variability in the genesis region and an additional maximum near 36°–38°N. However, the maximum standard deviation of SST is downstream of the maximum in the decadal mode described here and that described by Kwon and Deser (2007), indicating that internal oceanic dynamics are likely not responsible for the presence of the decadal mode of variability in CPL.

REFERENCES

Alexander, M. A., I. Bladé, M. Newman, J. R. Lanzante, N.-C. Lau, and J. D. Scott, 2002: The atmospheric bridge: The influence of ENSO teleconnections on air–sea interaction over the global oceans. *J. Climate,* **15,** 2205–2231.

——, and Coauthors, 2006: Extratropical atmosphere–ocean variability in CCSM3. *J. Climate,* **19,** 2496–2525.

Collins, W. D., and Coauthors, 2006: The Community Climate System Model Version 3 (CCSM3). *J. Climate,* **19,** 2122–2143.

Conkright, M. E., R. A. Locarnini, H. E. Garcia, T. D. O'Brien, T. P. Boyer, C. Stephens, and J. I. Antonov, 2002: *World Ocean Atlas 2001: Objective Analyses, Data Statistics, and Figures, CD-ROM Documentation*. National Oceanographic Data Center, 17 pp.

Danabasoglu, G., 2008: On multidecadal variability of the atlantic meridional overturning circulation in the Community Climate System Model version 3. *J. Climate,* **21,** 5524–5544.

Dawe, J. T., and L. Thompson, 2005: Viscosity-dependent internal variability in a model of the North Pacific. *J. Phys. Oceanogr.,* **35,** 747–756.

Deser, C., and M. L. Blackmon, 1995: On the relationship between tropical and North Pacific sea surface temperature variations. *J. Climate,* **8,** 1677–1680.

——, M. A. Alexander, and M. S. Timlin, 1999: Evidence for a wind-driven intensification of the Kuroshio Current Extension from the 1970s to the 1980s. *J. Climate,* **12,** 1697–1706.

Ducet, N., P.-Y. L. Traon, and G. Reverdin, 2000: Global high-resolution mapping of ocean circulation from TOPEX/Poseidon and ERS-1 and -2. *J. Geophys. Res.,* **105,** 19 477–19 498.

Gent, P. R., and J. C. McWilliams, 1990: Isopycnal mixing in ocean circulation models. *J. Phys. Oceanogr.,* **20,** 150–155.

——, and G. Danabasoglu, 2004: Heat uptake and the thermohaline circulation in the Community Climate System Model, version 2. *J. Climate,* **17,** 4058–4069.

——, S. G. Yeager, R. B. Neale, S. Levis, and D. A. Bailey, 2009: Improvements in a half-degree atmosphere–land version of the CCSM. *Climate Dyn.,* **34,** 819–833.

Hanawa, K., and L. D. Talley, 2001: Mode waters. *Ocean Circulation and Climate,* G. Siedler and J. Church, Eds., International Geophysics Series, Vol. 77, Academic Press, 373–386.

Hazeleger, W., and S. S. Drijfhout, 2000: A model study on internally generated variability in subtropical mode water formation. *J. Geophys. Res.,* **105,** 13 965–13 979.

Kelly, K. A., 1991: The meandering Gulf Stream as seen by the geosat altimeter: Surface transport, position, and velocity variance from 73° to 46°W. *J. Geophys. Res.,* **96,** 16 721–16 738.

——, M. J. Caruso, S. Singh, and B. Qiu, 1996: Observations of atmosphere–ocean coupling in midlatitude western boundary currents. *J. Geophys. Res.,* **101,** 6295–6312.

——, L. Thompson, W. Cheng, and E. J. Metzger, 2007: Evaluation of HYCOM in the Kuroshio Extension region using new metrics. *J. Geophys. Res.,* **112,** C01004, doi:10.1029/2006JC003614.

Knutson, T. R., and Coauthors, 2006: Assessment of twentieth-century regional surface temperature trends using the GFDL CM2 coupled models. *J. Climate,* **19,** 1624–1651.

Kobayashi, T., 1999: Study of the formation of North Pacific Intermediate Water by a general circulation model and the particle-tracking method 1. A pitfall of general circulation model studies. *J. Geophys. Res.,* **104,** 5423–5440.

——, 2000: Study of the formation of North Pacific Intermediate Water by a general circulation model and the particle-tracking method: 2. Formation mechanism of salinity minimum from the view of the ''critical gradient'' of the Oyashio mixing ratio. *J. Geophys. Res.,* **105,** 1055–1070.

Kwon, Y.-O., and C. Deser, 2007: North Pacific decadal variability in the Community Climate System model version 2. *J. Climate,* **20,** 2416–2433.

Large, W. G., and S. G. Yeager, 2004: Diurnal to decadal global forcing for ocean and sea ice models: The data sets and flux climatologies. NCAR Tech. Rep. TN-460+STR, 105 pp.

——, and G. Danabasoglu, 2006: Attribution and impacts of upper-ocean biases in CCSM3. *J. Climate,* **19,** 2325–2346.

Latif, M., and T. P. Barnett, 1996: Decadal climate variability over the North Pacific and North America: Dynamics and predictability. *J. Climate,* **9,** 2407–2423.

Maltrud, M., F. Bryan, and S. Peacock, 2010: Boundary impulse response functions in a century-long eddying global ocean simulation. *Environ. Fluid Mech.,* **10,** 275–295.

Mantua, N. J., S. R. Hare, Y. Zhang, J. M. Wallace, and R. Francis, 1997: A Pacific interdecadal climate oscillation with impacts on salmon production. *Bull. Amer. Meteor. Soc.,* **78,** 1069–1079.

Maximenko, N. A., and P. P. Niiler, 2004: Hybrid decade-mean global sea level with mesoscale resolution. *Recent Advances in Marine Science and Technology,* N. Saxena, Ed., PACON International, 55–59.

Nakamura, H., and A. S. Kazmin, 2003: Decadal changes in the North Pacific oceanic frontal zones as revealed in ship and satellite observations. *J. Geophys. Res.,* **108,** 3078, doi:10.1029/1999JC000085.

Nonaka, M., H. Nakamura, Y. Tanimoto, T. Kagimoto, and H. Sasaki, 2006: Decadal variability in the Kuroshio–Oyashio Extension simulated in an eddy-resolving OGCM. *J. Climate,* **19,** 1970–1989.

Pierce, D. W., T. P. Barnett, N. Schneider, R. Saravanan, D. Dommenget, and M. Latif, 2001: The role of ocean dynamics in producing decadal climate variability in the North Pacific. *Climate Dyn.,* **18,** 51–70.

Primeau, F., 2002: Multiple equilibria and low-frequency variability of wind-driven ocean currents. *J. Phys. Oceanogr.,* **32,** 2232–2256.

Qiu, B., 2000: Interannual variability of the Kuroshio Extension system and its impact on the wintertime SST field. *J. Phys. Oceanogr.,* **30,** 1486–1502.

——, 2003: Kuroshio Extension variability and forcing of the Pacific decadal oscillations: Responses and potential feedback. *J. Phys. Oceanogr.,* **33,** 2465–2482.

——, N. Schneider, and S. Chen, 2007: Coupled decadal variability in the North Pacific: An observationally constrained idealized model. *J. Climate,* **20,** 3602–3620.

Reynolds, R. W., T. M. Smith, C. Liu, D. B. Chelton, K. S. Casey, and M. G. Schlax, 2007: Daily high-resolution-blended analyses for sea surface temperature. *J. Climate,* **20,** 5473–5496.

Schneider, N., and A. J. Miller, 2001: Predicting western North Pacific Ocean climate. *J. Climate,* **14,** 3997–4002.

——, ——, and D. W. Pierce, 2002: Anatomy of North Pacific decadal variability. *J. Climate,* **15,** 586–605.

Seager, R., Y. Kushnir, N. H. Naik, M. A. Cane, and J. Miller, 2001: Wind-driven shifts in the latitude of the Kuroshio–Oyashio Extension and generation of SST anomalies on decadal timescales. *J. Climate,* **14,** 4149–4165.

Smith, T. M., R. W. Reynolds, T. C. Peterson, and J. Lawrimore, 2008: Improvements to NOAA's historical merged land–ocean surface temperature analysis (1880–2006). *J. Climate,* **21,** 2283–2296.

Talley, L. D., 1993: Distribution and formation of North Pacific intermediate water. *J. Phys. Oceanogr.,* **23,** 517–537.

——, 1997: North Pacific Intermediate Water transports in the mixed water region. *J. Phys. Oceanogr.,* **27,** 1795–1803.

Thompson, L., and W. Cheng, 2008: Water masses in the Pacific in CCSM3. *J. Climate,* **21,** 4514–4528.

Wu, L., D. E. Lee, and Z. Liu, 2005: The 1976/77 North Pacific climate regime shift: The role of subtropical ocean adjustment and coupled ocean–atmosphere feedbacks. *J. Climate,* **18,** 5125–5140.